Measurement 181 (2021) 109601

Contents lists available at ScienceDirect

Measurement

journal homepage: www.elsevier.com/locate/measurement

The assessment of metrological properties of segmental orifice based on simulations and experiments

Anna Golijanek-Jędrzejczyk [a,*], Andrzej Mrowiec [b], Robert Hanus [c], Marcin Zych [d], Marcin Heronimczak [e], Dariusz Świsulski [a]

[a] Gdańsk University of Technology, Faculty of Electrical and Control Engineering, 80-233 Gdańsk, Poland
[b] Calisia University, Polytechnic Faculty, 62-800 Kalisz, Poland
[c] Rzeszów University of Technology, Faculty of Electrical and Computer Engineering, 35-959 Rzeszów, Poland
[d] AGH University of Science and Technology, Faculty of Geology, Geophysics and Environmental Protection, 30-059 Kraków, Poland
[e] Calisia University, Medical-Social-Technical Faculty in Września, 62-800 Kalisz, Poland

ARTICLE INFO

Keywords:
Flow measurements
Segmental orifice
Mass flow
Uncertainty analysis
Flow simulation

ABSTRACT

Segmental orifices are often used to measure flows of heterogeneous mixtures, especially in flow meters in the power industry, for example. The orifice (with module $m = 0.25$) was installed in a stainless-steel pipe with internal diameter of 50 mm, placed in a hydraulic water system. The research was performed for Reynolds numbers ranging from 9,000 to 17,000. The flow characteristics of this orifice obtained based on simulation in SolidWorks Flow Simulation 2014 and experimental data were compared with standard-based calculations. It was determined that relative differences between the obtained flow characteristics did not exceed 1.5% for the experiment and 5.1% for the simulation. The article also presents the results of estimated uncertainty for mass flow measurement q_m using the analytical method and the Monte Carlo simulations. The results for both methods proved that the relative expanded uncertainty $U_{rel}(q_m)$ does not exceed 1.8% for the tested orifice.

1. Introduction

Modern technology uses various methods for measuring the mass flow rate, such as Coriolis flow meter [1–4] or thermal flow meters [5–6]. However, orifices are still one of the most frequently used flow measurement devices in the power, chemical, and mineral industry [7,8].

The simplicity of design and installation is their advantage, which turns them into highly reliable devices. Another advantage of orifices is their low cost of implementation and use [9]. The major disadvantages of this type of measurement are high pressure drop and high sensitivity to the inlet velocity profile in the orifice system.

Among the known designs of orifice plates, the standard (centric) orifice, whose accuracy is 1.5…2% in industrial systems [9], is most commonly used. When it is impossible to meet the flow conditions for fluids listed in the ISO 5167–1 standard, a non-standard orifice can be used, such as, for example, a quadrant edge orifice (particularly for flows at low Reynolds numbers), eccentric orifice, [10] or segmental orifice. The last two types of orifices are utilised primarily for fluids contaminated with solid particles that form suspensions. This type of flow occurs in the power industry [11]. Examples include flow measurements for coal dust suspensions in diesel or heating oil [12]. Despite the existing solutions, a simple, reliable and accurate flow measurement method is still being sought. The accuracy aspect is particularly difficult to be met because it is not easy to define the density of inhomogeneous mixture flowing through the Venturi flow meter. There have also been attempts to find new orifice solutions for fluid flow measurements that would be characterised by a constant value of discharge coefficient C in a wide range of Reynolds numbers [9,13].

The topics related to segmental orifices are of current interest due to their continuous application and use in the industry (e.g., in the power industry), where the flowing medium is a heterogeneous mixture. This type of orifice is commonly applied in coking plants. The problem is the lack of current standards for the use of this type of orifices. The current standard EN ISO 5167: 2003 [22,23] defines the following orifices: centric ISA, quadrant, eccentric, with conical inlet, Venturi tubes, and nozzles, as well as the methods of using them. Unfortunately, segmental orifices are not included. In Poland, one can refer to the earlier standard: the national PN-93/M−53950/01 [24], in which a lot of attention was paid to segmental orifices. This standard specifies the application ranges of the segmental orifice and provides calculation examples for water and

* Corresponding author.
E-mail address: anna.golijanek-jedrzejczyk@pg.edu.pl (A. Golijanek-Jędrzejczyk).

https://doi.org/10.1016/j.measurement.2021.109601
Received 10 February 2021; Received in revised form 10 May 2021; Accepted 12 May 2021
Available online 19 May 2021

Nomenclature

C	discharge coefficient [-]
C_e	experiment discharge coefficient [-]
C_s	simulation discharge coefficient [-]
D	pipe diameter [m]
a	slope [-]
b	intercept [-]
d	orifice diameter [m]
F_D	pipe cross-sectional area [m^2]
F_h	orifice cross-sectional area [m^2]
h	orifice clearance [mm]
k_p	coverage factor [-]
M	number of samples for Monte Carlo simulations [-]
m	orifice module [-]
N	number of input quantities for Monte Carlo simulations [-]
n	number of observations (measurements) [-]
p	pressure [Pa]
q_m	mass flow [kg/s]
q_{mc}	mass flow calculated from standard [kg/s]
q_{me}	experimental mass flow[kg/s]
q_{ms}	simulation mass flow[kg/s]
R^2	determination coefficient [-]
S	standard curve fitting error [-]
T	fluid (water)temperature [K]
t	time [s]
u	standard uncertainty [kg/s]
u_A	uncertainty Type A[kg/s]
u_B	uncertainty Type B [kg/s]
u_c	combined standard uncertainty [kg/s]
$U(q_m)$	mass flow expanded uncertainty [kg/s]
$U_{rel}(q_m)$	relative expanded uncertainty [%]
α	proportionality coefficient [$\sqrt{kg \cdot m}$]
β	orifice diameter ratio [-]
δl_e	relative error of shift between the calculated flow characteristics and the flow characteristics based on experimental data [%]
δl_s	relative error of shift between the calculated flow property and the flow property based on simulation data [%]
Δp	difference pressure [Pa]
γ	power coefficient [-]
ε	expansion coefficient [-]
ρ	fluid density[kg/m^3]
υ	velocity [m/s]

gas flows. However, with the adoption of international standards EN ISO 5167: 2003, this standard ceased to be a binding act. Moreover, there are only few publications on the study of segmental orifices in the literature. The tests of segmental orifices described in the literature concerned surface roughness changes in the orifice and the pipeline, or the inlet nozzles of curved surface, when measuring liquid–solid mixtures (as a result of the abrasive action of the mixture). The work [14] presents the results of laboratory and field tests concerning the measurement of flow of suspensions (liquids contaminated with sediment) in horizontal pipes with the use of measuring orifices. The relationship between the flow characteristics and the characteristics of liquid and solid phase components depending on the content of solids in the liquid was investigated. It was found that for the flow of suspensions through the orifice, its inlet edge changes (as the particles of the mixture settle), thus changing the geometry of the opening. Deposits also form in the pipe upstream and downstream of the orifice, which disturbs the flow kinematics. There are no such adverse effects in segmental orifices – thanks to their design, they do not pose an obstacle for solid particles moving in the mixture.

Mrowiec & Heronimczak [15] have considered the conditions concerning the influence of flow stability on the C coefficient of a segmental orifice. The authors presented the results of numerical simulations and experimental studies. The conducted analyses allowed to determine the minimum Reynolds number $Re = 10{,}000$, for which the C orifice factor can be assumed constant.

In turn, Straka et al. in [16] have presented studies of the influence of a 90° bend (commonly used structural element in piping systems) on the measurement accuracy of segmental flow meters with flow area of 7% of the pipeline area. The results of laser Doppler measurements made it possible to describe the flow structure in terms of changing the distance from 2 to 30 pipeline diameters.

In [18], the authors have reported the results of the research for a mixture of water and water-soluble oil (forming a white emulsion) which flows through the segmental orifice in different proportions of mineral oil to change the viscosity of the flowing emulsion at the throat coefficient of $\beta = 0.3$ and $\beta = 0.5$. It was concluded that the discharge coefficient at different oil concentrations is nearly the same, while the discharge coefficient decreases with increasing beta ratio.

The literature is also relatively scarce in terms of numerical simulations for segmental orifices. Straka et al. [17] have done a numerical investigation of segmental orifices using the stress-blended eddy simulation model (SBES) instead of the regular Reynolds-averaged Navier-Stokes (RANS) method to finely capture the details of turbulence in the orifice flow meter. The SBES model is a hybrid combination of RANS and LES (large eddy simulation) models. The obtained results indicated the superiority of the hybrid SBES model over the standard k-RANS model in segmental orifice simulation. The research results were verified by a large number of laser Doppler anemometry (LDA) and ultrasonic flowmeter measurements. It was found that near the orifice, SBES even has an advantage over LDA in predicting the ultrasonic meter performance.

To sum up, single publications can be found in the world literature that describe such issues of segmental orifice operation as surface roughness changes in the orifice, the impact of a 90° elbow, and flows of emulsion-type liquids through the orifice. However, the authors did not come across any simulation and experimental studies on the possibilities of using a segmental orifice in the developing turbulent water flow which would describe orifice's properties and analyse its accuracy of flow measurement. This observation was the motivation for the authors to study the segmental orifice.

The objective of the research described in this article was to analyse hydraulic and metrological properties of the selected segmental orifice. Simulations and experiments were carried out to check the changes in the value of mass flow, discharge coefficient and uncertainty of mass flow measurement in the area of turbulent flow, but at a relatively low Reynolds number, in the range of 9,000…17,000. The conducted numerical tests allowed to visualize the recirculation zones and study complex flow phenomena in this area, which was of key importance for determining the scope of segmental orifice application. Moreover, the corresponding experimental studies made it possible to validate the numerical results.

The article is divided into the following sections. Section 2 presents the tested segmental orifice and its parameters. The results of flow simulations through the segmental orifice for various mass flow rates are shown in Section 3. Section 4 presents the measuring devices used in the experiment and describes the findings of experimental tests with estimations of their measurement uncertainties. This section also includes a comparison study of the simulation and experiment results. Section 5 presents the summary and conclusions from the analysis.

2. Tested orifice

The simulation and experimental studies of the selected segmental orifice were performed as part of the tasks described herein. The experiments were carried out on a laboratory stand constructed at the President Stanislaw Wojciechowski Academy in Kalisz. The simulations were done in the SolidWorks Flow Simulation 2014.

The experiments were conducted on a closed-circuit hydraulic experimental stand [9] for seven different mass flow rates ranging from 0.35 kg/s to 0.63 kg/s, which corresponds to Reynolds numbers in the range of 9,920 to 16,270. The diagram of the measurement pipe section with the segmental orifice is shown in Fig. 1.

The tested orifice, made of 2.5 mm-thick stainless steel, had the clearance of $h = 15$ mm. Fig. 2 shows the main view of the analysed orifice.

This orifice is characterised by module m, i.e., the ratio of the hole area F_h to the pipe cross-sectional area F_D [19] (diameter ratio β):

$$m = \beta^2 = \frac{F_h}{F_D} \tag{1}$$

For the analysed orifice, the parameter m is equal to 0.25.

3. Numerical simulations

Numerical simulations of the measurement section of the hydraulic installation shown in Fig. 1 were performed as part of the segmental orifice tests in the SolidWorks Flow Simulation 2014 computing environment [20].

The simulation studies aimed to determine the places and scope of complex flow phenomena taking place downstream of the segmental orifice and mainly considered as disturbances. The analysis of the publications available on this subject shows that most frequently, the carried-out simulations refer to the flow through the centric orifice.

The results of the simulations were expected to provide data for selecting parameters for the experiment to be performed, for which the abovementioned disturbances would be as low as possible. It is important to ensure the stability of the liquid flow when taking measurements.

The used SolidWorks engineering software has the option to choose one of three flow models laminar, laminar-turbulent, and turbulent. The authors chose the turbulent model, along with the following boundary conditions: absolute static pressure of 150 kPa at inlet, and mass flow rate in kg/s at outlet. The selected pressure value corresponded to real conditions in the experimental installation.

The SolidWorks Flow Simulation uses orthogonal grid of finite volumes. The grid elements are cuboids with sides parallel to the base planes. In this case, the generated numerical grid consists of single cells of variable volumes. It becomes denser around the numerical orifice, where a 0.5 mm × 0.5 mm × 0.33 mm cell is obtained from a single 0.5 mm × 0.5 mm × 9 mm element. The 'Small Solid Feature Refinement Level' option has been used for better representation of details. In total, the computational grid consisted of 5,576,144 individual cuboids.

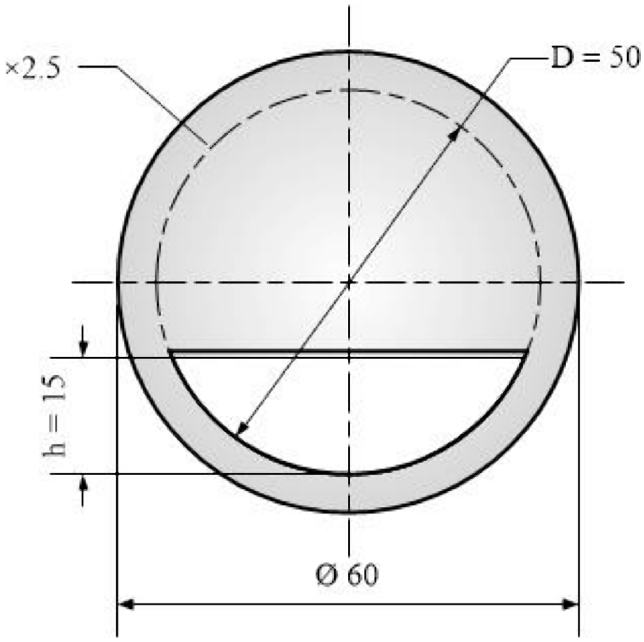

Fig. 2. View of segmental orifice.

In the simulation tests, the assumed mass flow rates q_m of the flowing water ranged from 0.35 kg/s to 0.65 kg/s, which corresponded to Reynolds numbers in the range from 9,860 to 16,580, thus simulating the turbulent flow. The water temperature was set at 20 °C, while the values of density and dynamic viscosity of water were taken from the built-in software library.

Fig. 3a-3c present selected simulation results showing static pressure distributions in the water flow through the segmental orifice. The distributions are presented along the axial section of the test system for three mass flow rates: $q_m = 0.35$ kg/s, $q_m = 0.45$ kg/s and $q_m = 0.65$ kg/s.

The maps of static pressure distribution shown in Fig. 3 reveal a sudden pressure difference in the narrowing area, upstream and downstream of the orifice. This pressure difference is the measured impact pressure on the tested orifice. For the mass flow rates: $q_m = 0.35$ kg/s, $q_m = 0.45$ kg/s and $q_m = 0.65$ kg/s, the following pressure differences were measured: $\Delta p = 600$ Pa, $\Delta p = 990$ Pa, and $\Delta p = 2080$ Pa, respectively.

The results obtained in the simulation allowed to estimate the

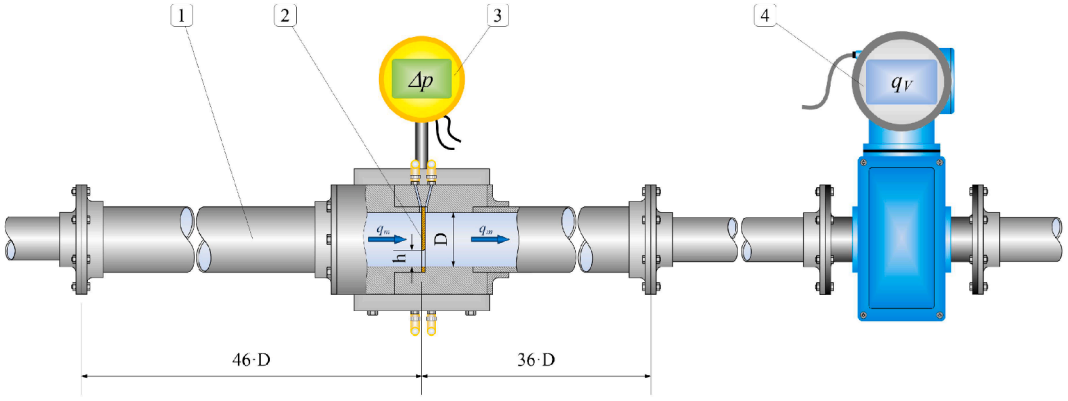

Fig. 1. Fragment of the hydraulic experimental installation: 1 – measurement pipe section with internal diameter $D = 50$ mm, 2 – tested segmental orifice, 3 – differential pressure transmitter APR-2000/ALW, 4 –electromagnetic flow meter PROMAG 30AT15.

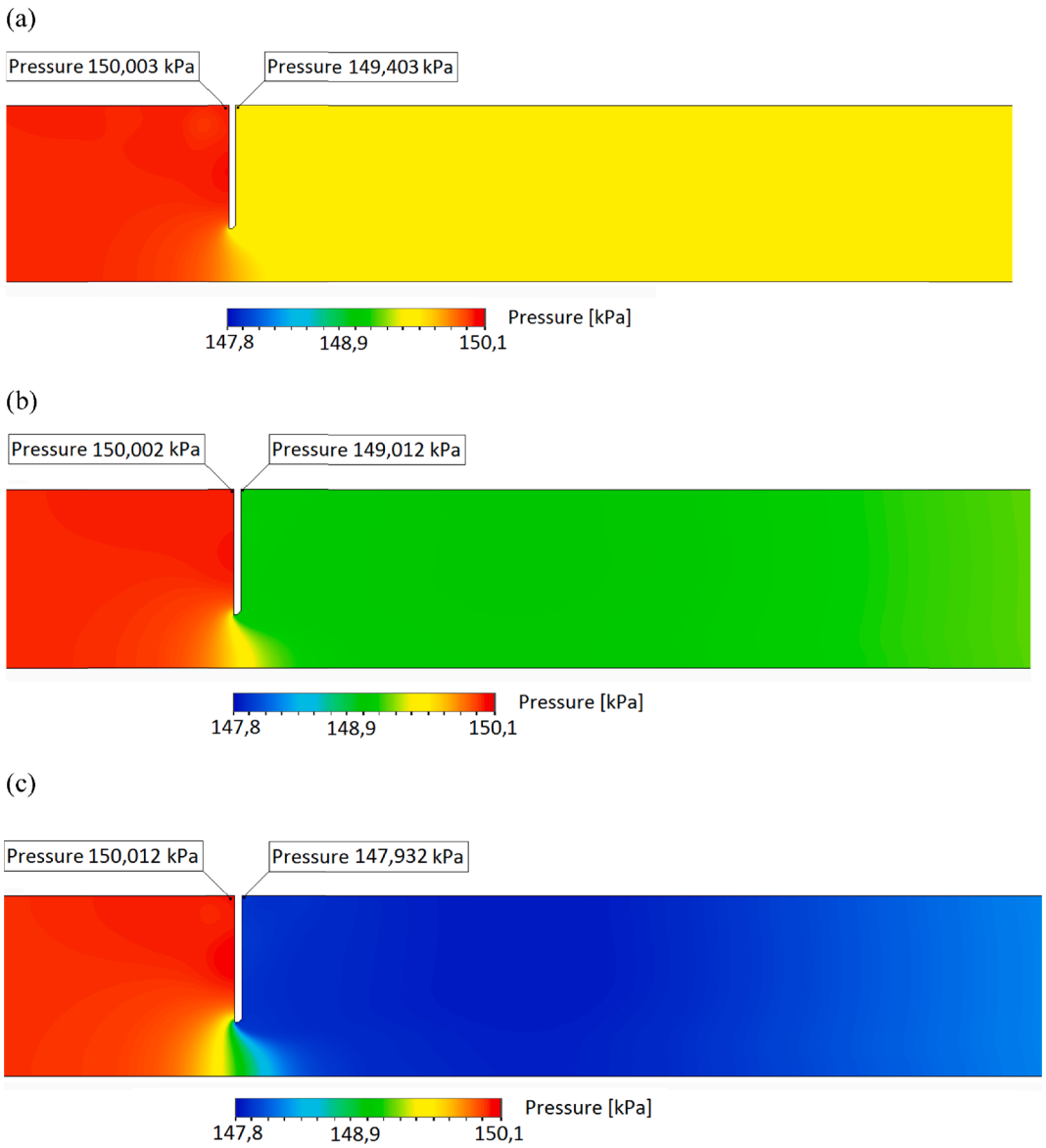

Fig. 3. Static pressure distributions in the longitudinal cross-section of the measurement section: (a) $q_m = 0.35$ kg/s, (b) $q_m = 0.45$ kg/s, (c) $q_m = 0.65$ kg/s.

desired minimum pressure setting in the transmitter used for the experiment. This way, a properly measuring transmitter could be chosen. In the analysed case, the pressure difference was 2.1 kPa for the maximum simulated mass flow rate q_m.

Fig. 4a-4c show maps of velocity distributions in the form of rainbows of colours, with velocity vectors placed in the tested segmental orifice area for the same values of mass flow rate q_m.

For the analysed flows: $q_m = 0.35$ kg/s, $q_m = 0.45$ kg/s and $q_m = 0.65$ kg/s, the water velocity downstream of the orifice narrowing increased to 1.13 m/s, 1.45 m/s and 2.1 m/s, respectively.

As a result of the simulation, it was observed that in the orifice area, the structure of the fluid downstream of the orifice undergoes great deformation and then turns again into that of the free flow. In this area, there is some pressure loss caused by the formation of vortices (characteristic direction changes of velocity vectors can be observed). The analysis of the disturbance zone caused by the orifice made it possible to place the electromagnetic flowmeter at an appropriate distance in the experiment to ensure its stable operation.

In addition to the maps shown in Fig. 3 and Fig. 4, the simulation in SolidWorks Flow Simulation allowed to determine the flow characteristics of the tested orifice, as presented in Section 4.1.

Certainly, numerical analyses of liquid flow through orifices which are reported in the literature frequently use more advanced software, e. g. ANSYS Fluent, equipped with a dozen or so calculation models that allow the user to select a relevant computational grid and thus obtain more accurate results.

The authors of the present study started with a simpler tool, the SolidWorks Flow Simulation environment. The calculations performed in this environment were very helpful in designing experimental tests, including determining the measuring range of the pressure difference converter depending on the mass flow rate of the flowing liquid.

The disturbances in the liquid flow through the segmental orifice are related with the fact that the liquid flows only through the segment of the circle in the orifice, which is characteristic of this type of flow meter. Fig. 4 clearly shows the effect of flow choking and the resulting flow stability disturbances just behind the baffle in the pipeline on the downstream side of the orifice. The presented velocity profiles indicate that significant flow disturbances (colours from red to green) almost totally disappear at a distance of 5·D downstream of the orifice.

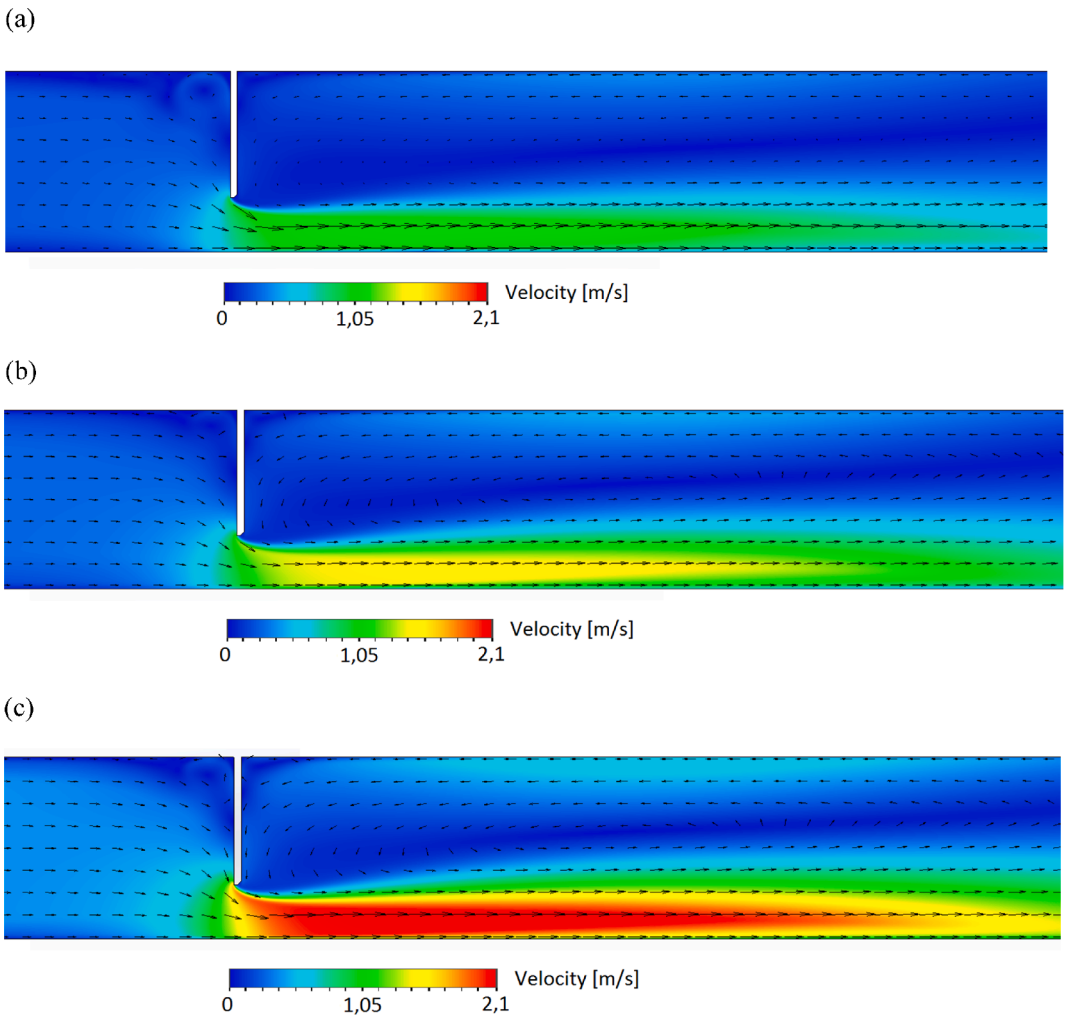

Fig. 4. Velocity distribution maps in the longitudinal cross-section: (a) $q_m = 0.35$ kg/s, (b) $q_m = 0.45$ kg/s, (c) $q_m = 0.65$ kg/s.

4. Experimental research

Section 4 presents the results of experimental tests of the prototype segmental orifice carried out on a hydraulic stand. Since the measurement results cannot be compared without a qualitative evaluation of the measurements, the full uncertainty analysis of the mass flow measurement through this orifice was also carried out. Carrying out both the simulation and the experiment is of particular importance, as it makes it possible to compare the obtained results.

The structure of the hydraulic experimental stand is the same as that described in [9]. The studied segmental orifice (Fig. 2) was placed in a smooth stainless-steel pipe (with inner diameter $D = 50$ mm) at a distance of 2.3 m ($46 \cdot D$) upstream and 1.8 m ($36 \cdot D$) downstream of the orifice plate (Fig. 1).

Based on the conclusions from the simulation of the impact pressure difference on the segmental orifice, the APR-2000/ALW transmitter with standard current output and the measuring range set to $\Delta p = 0$–2.4 kPa (time constant $t = 5$ s) was selected for use.

The electromagnetic flow meter PROMAG 30AT15 was utilised as the reference meter. This instrument was set to the measuring range of 1.0 dm^3/s of the volumetric flow at 21 °C. The measured volumetric flow rates were automatically converted into mass flow rates, with consideration to temperature dependent changes of flowing fluid density.

The mass flow measurements were made for a stabilised water flow, which was gradually adjusted through a replaceable discharge throttle. 30 measurements were taken and then averaged for each stabilised flow rate. The performed measurements included mass flow rate of water, differential impact pressure, and fluid temperature. The flow characteristic obtained in this way is presented in Section 4.1. For all recorded measurements series, the average temperature ranged from 20.7 °C to 24.8 °C, and for each series, the temperature change did not exceed 2.0 °C.

4.1. Mass flow rate measurement

The mass flow rate q_m of the fluid flowing through the tested segmental orifice is given by theoretical equation (2) [21–23]:

$$q_m = \frac{C \cdot \varepsilon \cdot F_h}{\sqrt{1 - m^2}} \cdot \sqrt{2 \cdot \Delta p \cdot \rho} \tag{2}$$

Bearing in mind that the orifice module m for the circular cross-section is given by equation (1), after substituting formula (1) to equation (2), the following formula is obtained for the mass flow rate of an incompressible fluid (for water $\varepsilon = 1$) flowing through the segmental orifice:

$$q_m = \frac{C \cdot F_h}{\sqrt{1 - \left(\frac{F_h}{F_D}\right)^2}} \cdot \sqrt{2 \cdot \Delta p \cdot \rho} \tag{3}$$

Then the mass flow rate q_m can be determined indirectly, and the measurement function depends on the following parameters: $q_m = f(C, F_h, F_D, \Delta p, \rho)$.

In practice, with stabilised flow parameters, equation (3) can be converted to the form:

$$q_m = \alpha \cdot \Delta p^{\gamma} \tag{4}$$

where, from the fluid flow theory:

$$\alpha = \frac{C \cdot F_h}{\sqrt{1 - \left(\frac{F_h}{F_D}\right)^2}} \cdot \sqrt{2 \cdot \rho} \tag{5}$$

and: $\gamma = 0.5$.

The characteristic of $q_{mc} = \alpha \cdot \Delta p^{\gamma}$ calculated according to standard [24] for the examined orifice is shown in Fig. 5. This characteristic can be described by the equation:

$$q_{mc} = 0.0136 \cdot \Delta p^{0.5} \mathrm{q_m} = 0.0136 \cdot \Delta \mathrm{p}^{0.5} \tag{6}$$

Further sections of the article show the results obtained from the simulations with SolidWorks Flow Simulation 2014 and from the experiments conducted at the laboratory stand. To distinguish more easily between the mass flow rates obtained from simulation and experiment, they are marked as q_{ms} and q_{me}, respectively.

Table 1 and Fig. 5 show the results of SolidWorks simulations for the increasing values of differential pressure Δp at a given mass flow rate q_{ms}. The flow values shown in Fig. 5 were calculated based on the theory of flows and simulations in SolidWorks.

Table 2 presents the flow characteristic (for mass flow rate q_{mc}) calculated as per standard [24] for the values of difference pressure Δp obtained experimentally.

The error bars on the calculation curve q_{mc} specify the errors calculated based on the standard [24].

The exact equation describing the simulation data-based function $q_{ms} = \alpha \cdot \Delta p^{\gamma}$ is as follows:

$$q_{ms} = 0.0143 \cdot \Delta p^{0.501} \tag{7}$$

The standard curve fitting errors (understood as relative errors for a given pressure, being the differences between the mass flow rates from the simulation and from formula (7)) are, respectively: $S_\alpha = 1.2\ 10^{-4}\ \sqrt{kg \cdot m}$ for coefficient α, and $S_\gamma = 1.2 \cdot 10^{-3}$ for the exponent. In this case, the coefficient of determination R^2 is 0.99997.

The experimental results for the tested orifice are shown in Table 3 and Fig. 6. The mass flow rates q_{me} were calculated from the measurements using the electromagnetic flow meter PROMAG 30AT15.

The error bars on the calculation curve q_{mc} specify the absolute errors based on the standard (the same way as in Fig. 5). For the experimental characteristic q_{me}, these errors resulted from the indication error, which for the electromagnetic flow meter PROMAG 30AT15is equal to $\pm(0.2\% \cdot q_{\mathrm{measured}} + 0.05\% \cdot 1)$ [kg/s].

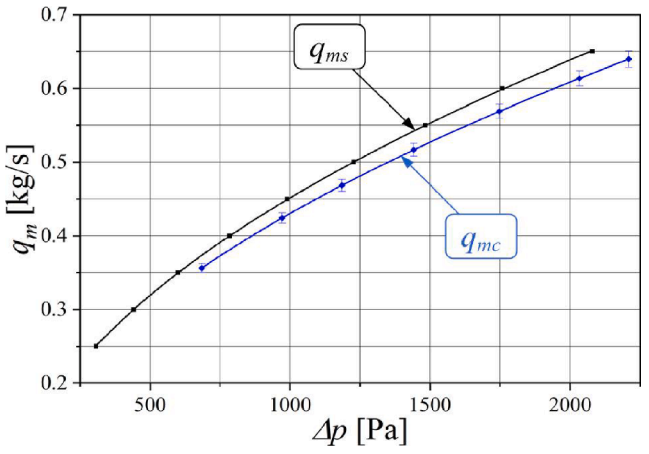

Fig. 5. Flow characteristics of the segmental orifice: q_{mc} – calculated according to the standard [24], q_{ms} – obtained from simulations in SolidWorks environment.

For the experimental data, the exact equation describing the function $q_{me} = \alpha \cdot \Delta p^{\gamma}$ is as follows:

$$q_{me} = 0.0131 \cdot \Delta p^{0.504} \tag{8}$$

The standard curve fitting errors in this case are: $S_\alpha = 2.6 \cdot 10^{-4} \sqrt{kg \cdot m}$ for coefficient α, and

$S_\gamma = 2.7 \cdot 10^{-3}$ for the exponent, respectively, while the coefficient of determination is

$R^2 = 0.99984$.

Analysing the characteristics given by equations (7) and (8), it was found that the obtained exponents are slightly greater than the values obtained based on the standard (formula (6)). This is confirmed by the fact that in engineering practice, the exponent value oscillates around 0.5. The present research has shown that the characteristics of the experimental and simulation data slightly differ from the calculations performed according to the standard.

Trend equations were used to set appropriate values of the flowing water in the tested range of impact pressure changes in the orifice. Then, to compare the characteristics, the relative measures of their shift were determined as:

$$\delta l_e = \frac{|q_{me} - q_{mc}|}{q_{mc}} 100\% \tag{9}$$

$$\delta l_s = \frac{|q_{ms} - q_{mc}|}{q_{mc}} 100\% \tag{10}$$

Diagrams of δl_e and δl_s relations with Δp (in the analysed range of Δp) are shown in Fig. 7.

Based on the obtained results, it can be concluded that the values of δl_e do not exceed 1.5%, which proves very good convergence of experimental and computational data. The values of δl_s are in the range of 5% to 5.1%, which is acceptable in engineering practice. The maximum relative difference in the mass flow rate between the experimental and simulation data does not exceed 6.5% in the tested range of Δp. This last value results from negative values of differences $(q_{me} - q_{mc})$ in formula (9).

To check the similarity between the sets of points obtained experimentally and then calculated according to the theory of fluid mechanics, and those obtained from simulations, cross plots were drawn, which are shown in Figs. 8-10. Since the modelling points and the experimental points did not overlap, the points for the graphs were determined from the fit function described by equation (7). Therefore, the uncertainty points were calculated from the law of uncertainty propagation, based on curve fitting errors. Table 4 summarizes the parameters of the fitted lines obtained by the least-squares method and the errors of matching the coefficients: a (slope) - S_a, and b (intercept) - S_b.

Analyzing the data in Table 4 and the graphs in Figs. 8-10 leads to the conclusion that there is a linear relationship between all data sets, as evidenced by the Pearson's R^2 coefficient equal or close to 1.

The greatest agreement in the studied range occurs between the experimental data and the data obtained from the theoretical relationship (6). This is indicated by the slope values in the fit error limit equal to 1 and the intercept close to 0. In this respect, the comparison with the values obtained from the modeled curve is worse. In both cases, when compared with the experiment and with the theoretical curve, the coefficient a is close to 1, but not within the fit error limit. On the other hand, the coefficient b is also close to 0.

Hence, the slope is decisive for data convergence in all considered cases. Based on this, it can be concluded that the simulation model will show the greatest compliance with both the experiment and the theoretical curve for low flow values. As the flow rate increases, this compliance decreases (Fig. 5). Therefore, it should be stated that the

Table 1
Mass flow rates q_{ms} obtained from simulation.

q_{ms}[kg/s]	0.2500	0.3000	0.3500	0.4000	0.4500	0.5000	0.5500	0.6000	0.6500
Δp [Pa]	308	443	600	784	990	1228	1483	1758	2080

Table 2
Mass flow rates q_{mc} calculated according to the standard [24] for experimentally obtained values of difference pressureΔp.

q_{mc}[kg/s]	0.3562	0.4242	0.4685	0.5168	0.5689	0.6138	0.6397
Δp [Pa]	685	971	1185	1442	1747	2034	2209

Table 3
Mass flow rates $q_{me}(\Delta p)$ obtained experimentally.

q_{me}[kg/s]	0.3511	0.4222	0.4659	0.5147	0.5662	0.6106	0.6362
Δp [Pa]	685	971	1185	1442	1747	2034	2209

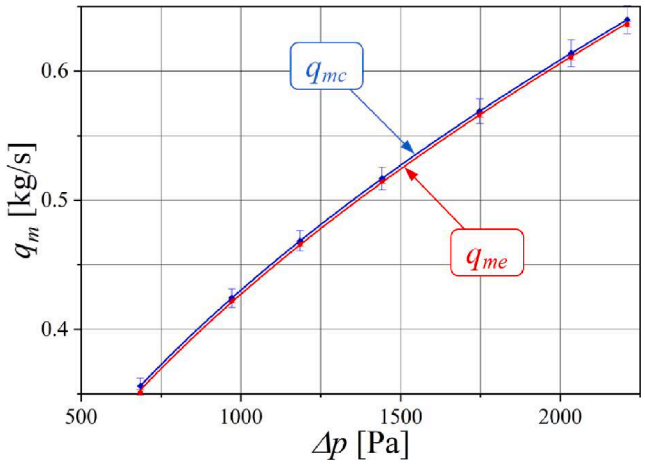

Fig. 6. Flow characteristics of the tested segmental orifice: q_{mc} – calculated from the standard [23], q_{me} – obtained experimentally.

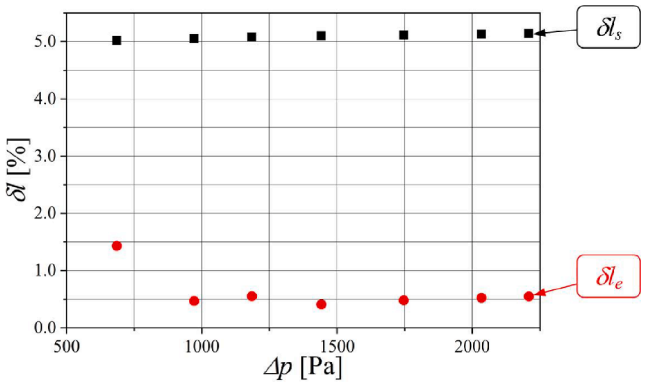

Fig. 7. Shifts δl_e and δl_s as functions of Δp.

relationship (3) obtained from the standards: EN ISO 5167–1: 2003 and EN ISO 5167–2: 2003 (within the limit of the assumed flux measurement uncertainty) describes well the flow characteristics of the segmental orifice in the tested range. In this respect, further work on the simulation model for this type of orifice should be carried out.

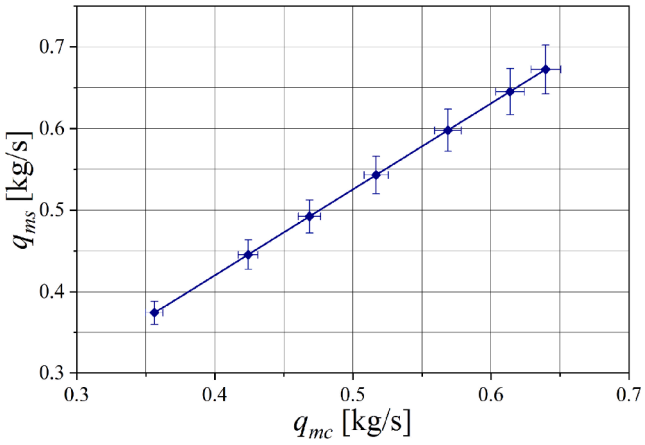

Fig. 8. Comparison of datasets obtained from the theoretical curve and from modelling in the SolidWorks Flow Simulation environment.

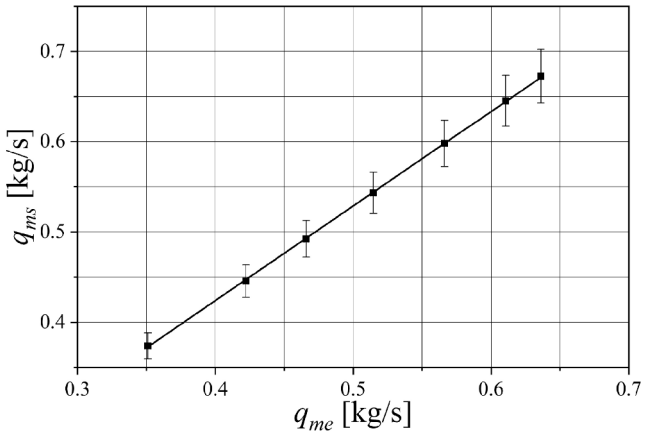

Fig. 9. Comparison of datasets obtained experimentally and from modelling in the SolidWorks Flow Simulation environment.

4.2. Estimating uncertainty of mass flow rate measurement

The presentation of full information on the results of mass flow rate measurements requires estimating measurement uncertainties.

The objective of the research presented in this section was to

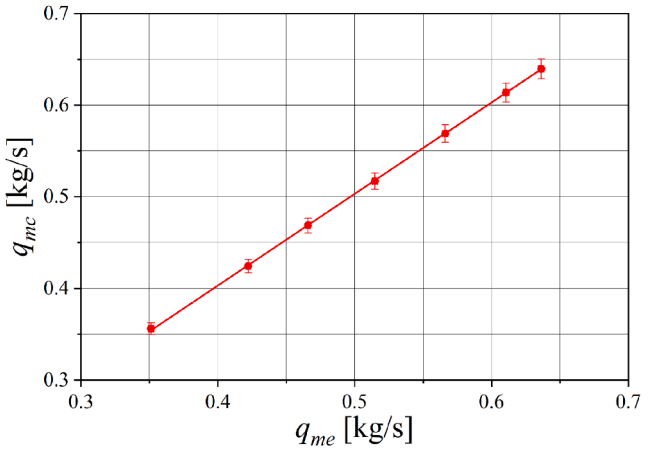

Fig. 10. Comparison of datasets obtained experimentally and from the theoretical curve.

Table 4
List of parameters for fitting straight lines to cross plots (Figs. 8-10).

Number of plot	R^2	a [-]	b [-]	S_a [-]	S_b [-]
Fig. 8	1.00000	1.0529	−0.0010	0.0001	0.0001
Fig. 9	0.99987	1.0504	0.0035	0.0048	0.0025
Fig. 10	0.99992	0.9975	0.0043	0.0044	0.0023

estimate the expanded uncertainty $U(q_m)$ of mass flow rate for the coverage factor $k_p = 2.00$ (corresponding to the confidence level equal to 0.95). The analyses were carried out using both the analytical method (as per [25–27]) and the Monte Carlo method, while adopting the following assumptions:

- fluid flow continuity and velocity uniformity are maintained at any point of any cross-section perpendicular to the flow axis,
- the fluid is incompressible, with no internal friction, and has constant density ρ (fluid density upstream and downstream of the orifice is the same),
- 30 measurements were made in series to obtain seven observation points of the average flow q_m.

Knowing that the mass flow rate q_m for the segmental orifice is given by equation (3), and assuming no correlation between the uncertainties of measured quantities (according to the law of the uncertainty propagation [24–25]), the combined uncertainty $u_c(q_{mc})$ can be presented as follows [7]:

$$u_c(q_{mc}) = \sqrt{u_A^2(q_{mc}) + \left(\frac{\partial q_{mc}}{\partial C}\right)^2 \cdot u^2(C) + \left(\frac{\partial q_{mc}}{\partial F_h}\right)^2 \cdot u^2(F_h) + \left(\frac{\partial q_{mc}}{\partial F_D}\right)^2 \cdot u^2(F_D) + \left(\frac{\partial q_{mc}}{\partial \Delta p}\right)^2 \cdot u^2(\Delta p) + \left(\frac{\partial q_{mc}}{\partial \rho}\right)^2 \cdot u^2(\rho)} \quad (11)$$

where $u_A(q_m)$ is the Type A uncertainty, $\frac{\partial q_{mc}}{\partial C}, \frac{\partial q_{mc}}{\partial F_h}, \frac{\partial q_{mc}}{\partial F_D}, \frac{\partial q_{mc}}{\partial \Delta p}, \frac{\partial q_{mc}}{\partial \rho}$ are the partial derivatives and $u^2(C)$, $u^2(F_h)$, $u^2(F_D)$, $u^2(\Delta p)$, $u^2(\rho)$ are the variances determined based on type B uncertainty.

Firstly, the partial derivatives in equation (11) were defined, see Table 5.

The next step was to determine all variances in formula (11), i.e., $u^2(C)$, $u^2(F_h)$, $u^2(F_D)$, $u^2(\Delta p)$ and $u^2(\rho)$.

The variation $u^2(C)$ of discharge coefficient is related to the measurement uncertainty for coefficient C. This uncertainty was determined as per standard [23], based on the relative measurement uncertainty $U(C)/C = 1.39\%$ and the coverage factor $k_p = 2$:

$$u(C) = \frac{U(C) \cdot C}{k_p} \quad (17)$$

The variances $u^2(F_h)$ and $u^2(F_D)$ related to the narrowing cross-section areas: F_h of the orifice and F_D of the pipe, respectively, were determined as type B variance [24] (assuming relative measurement uncertainty equal to 0.7% for each of these areas, and rectangular probability distribution).

The variance $u^2(\Delta p)$ of pressure measurement was also calculated as type B variance [25]. The maximum relative measurement error for the differential pressure is 0.15% (for the measuring range of 2.4 kPa). The rectangular probability distribution of this error was also assumed.

The variance $u^2(\rho)$ of fluid density was estimated as type B uncertainty, assuming the maximum absolute error of density measurement equal to 0.5 kg/m^3 (with temperature change in the measurement series not exceeding 2 °C), and the rectangular probability distribution of this error.

Finally, after calculating the combined mass flow rate uncertainties $u_c(q_m)$, the expanded uncertainty $U(q_m)$ was determined as:

$$U(q_m) = k_p \cdot u_c(q_m) \quad (18)$$

Analysing the expanded mass flow rate uncertainty $U(q_{mc})$ obtained for $k_p = 2$, it was found that for the smallest mass flow rate $q_{me} = 0.3511$ kg/s, the value of the expanded uncertainty $U(q_{mc})$ of flow measurement was 0.0063 kg/s (Table 6). The maximum value of $U(q_{mc}) = 0.0108$ kg/s was obtained for the highest mass flow rate q_{mc} of 0.6362 kg/s (Fig. 8). The highest value of the relative expanded uncertainty $U_{rel}(q_{mc})$ was 1.79% and occurred for the lowest tested mass

Table 5
Formulas for partial derivatives in equation (11).

Partial Derivatives	Formula	
$\frac{\partial q_{mc}}{\partial C}\left[\frac{kg}{s}\right]$	$\frac{F_h \cdot \sqrt{2 \cdot \Delta p \cdot \rho}}{\sqrt{1 - \left(\frac{F_h}{F_D}\right)^2}}$	(12)
$\frac{\partial q_{mc}}{\partial F_h}\left[\frac{kg}{m^2 \cdot s}\right]$	$\frac{\sqrt{1 - \left(\frac{F_h}{F_D}\right)^2} + \left(\frac{F_h}{F_D}\right)^2 \cdot \frac{1}{\sqrt{1 - \left(\frac{F_h}{F_D}\right)^2}}}{C \cdot \sqrt{2 \cdot \Delta p \cdot \rho} \cdot \frac{}{1 - \left(\frac{F_h}{F_D}\right)^2}}$	(13)
$\frac{\partial q_{mc}}{\partial F_D}\left[\frac{kg}{m^2 \cdot s}\right]$	$\frac{-C \cdot F_h^3 \cdot \sqrt{2 \cdot \Delta p \cdot \rho}}{F_D^3 \cdot \left(\sqrt{1 - \left(\frac{F_h}{F_D}\right)^2}\right)^{\frac{3}{2}}}$	(14)
$\frac{\partial q_{mc}}{\partial \Delta p}[m \cdot s]$	$\frac{C \cdot F_h}{\sqrt{1 - \left(\frac{F_h}{F_D}\right)^2}} \frac{\rho}{\sqrt{2 \cdot \Delta p \cdot \rho}}$	(15)
$\frac{\partial q_{mc}}{\partial \rho}\left[\frac{m^2}{s}\right]$	$\frac{C \cdot F_h}{\sqrt{1 - \left(\frac{F_h}{F_D}\right)^2}} \cdot \frac{\Delta p}{\sqrt{2 \cdot \Delta p \cdot \rho}}$	(16)

Table 6
Values of absolute and relative expanded uncertainty calculated analytically: $U(q_{mc})$, $U_{rel}(q_{mc})$, and simulated with the Monte Carlo method: $U_{MC}(q_{mc})$, $U_{relMC}(q_{mc})$.

Re [-]	$U(q_{mc})$ [kg/s]	$U_{rel}(q_{mc})$ [%]	$U_{MC}(q_{mc})$ [kg/s]	$U_{relMC}(q_{mc})$ [%]
9887	0.0063	1.79	0.0062	1.77
11,732	0.0072	1.71	0.0070	1.66
12,257	0.0080	1.72	0.0078	1.67
13,642	0.0088	1.71	0.0084	1.63
14,868	0.0096	1.70	0.0094	1.66
15,916	0.0104	1.70	0.0101	1.65
16,226	0.0108	1.70	0.0106	1.67

flow rate $q_{me} = 0.3511$ kg/s.

In addition to the analytical calculations of measurement uncertainty for mass flow rate q_{mc}, the Monte Carlo (MC) simulation was also conducted to verify the numerical calculation results. The procedure was identical to that described in [9,27]. The analyses were performed in Microsoft Excel for seven different values of mass flow rate q_m, the same as in the laboratory experiment, and for the number of samples $M = 10^4$. The results of estimation of the expanded uncertainty $U_{MC}(q_{mc})$ obtained using the MC method are presented in Table 6.

To further compare the theoretical, experimental and simulation results, the uncertainty analysis was also carried out based on the experimental and simulation calibration curves given by relations (7) - (8). Using the law of uncertainty propagation, the following formula was obtained for the combined uncertainty:

$$u_c(q_{me}) = \sqrt{(\Delta p^{\gamma} \cdot S_{\alpha})^2 + (\alpha \cdot \gamma \cdot \Delta p^{\gamma-1} \cdot u(\Delta p))^2 + (\alpha \cdot \Delta p^{\gamma} \cdot ln(\Delta p) \cdot S_{\gamma})^2} \quad (19)$$

Similarly, to the uncertainties calculated from the theoretical formula (3), the expanded uncertainties $U(q_{me})$, $U(q_{ms})$ and the relative expanded uncertainties $U_{rel}(q_{me})$, $U_{rel}(q_{ms})$ were estimated. The obtained values are shown in Table7. A comparison of the expanded uncertainties obtained with all analysed methods is shown in Fig. 11.

Analysis of Tables 6 and 7 and the graph in Fig. 11 shows that for all analysed methods the expanded uncertainty increases with increasing Reynolds number *Re*. Such a tendency is related to the increase of turbulence in the flow, and consequently, the disturbance in the flow caused by the orifice under investigation is greater. This is illustrated by the velocity vector distribution maps (Fig. 4a – 4c). The highest values of $U(q_m)$ are obtained from the calibration curve obtained by simulation in SolidWorks environment. Such high values of $U_{rel}(q_{ms})$ in the range of 3.87% to 4.43% are caused by the lower accuracy of the simulation to experiment and theory.

The uncertainties calculated from the experimental calibration curve, on the other hand, are subject to a dispersion of measurement points. This dispersion is mainly because it was not possible to maintain the same measuring conditions (temperature, external pressure). Taking into account that the dispersion is not large, it should be considered that the obtained values of $U_{rel}(q_{me})$ in the range of 2.25% to 2.42% are real, limiting values, which should not be exceeded if the orifice is properly installed and operated.

The uncertainty values obtained from the analysis of the theoretical relation (3) and the Monte Carlo simulation show the lowest values and are close to each other. Whereby, $U_{rel}(q_{mc})$ varies in the range from 1.70% to 1.79% and $U_{relMC}(q_{mc})$ in the range from 1.67% to 1.77%. These uncertainty values should be considered the lowest achievable for measurements with segmented orifices for $Re = 9{,}887 - 16{,}226$.

4.3. Analysis of the discharge coefficient C value

Analysing the results of experimental observations and simulations, it was found that for the segmental orifice, the values of the discharge coefficient C_e(experiment) and C_s(simulation), change with Reynolds number as shown in Fig. 12.

Table 7
Values of absolute and relative expanded uncertainty calculated from experimental -$U(q_{me})$, $U_{rel}(q_{me})$, and simulation - $U(q_{ms})$, $U_{rel}(q_{ms})$ calibration curves.

Re [-]	$U(q_{me})$ [kg/s]	$U_{rel}(q_{me})$ [%]	$U(q_{ms})$ [kg/s]	$U_{rel}(q_{ms})$ [%]
9887	0.0084	2.25	0.0145	3.87
11,732	0.0102	2.30	0.0180	4.03
12,257	0.0114	2.32	0.0203	4.12
13,642	0.0128	2.35	0.0229	4.22
14,868	0.0142	2.38	0.0258	4.31
15,916	0.0155	2.41	0.0283	4.39
16,226	0.0163	2.42	0.0298	4.43

The constant value of the discharge coefficient C_c for the tested orifice, represented as a solid line in the diagram in Fig. 12, was calculated (based on [24]) from the equation:

$$C_c = \sqrt{1 - \beta^4} \cdot (0.6057 + 0.2214 \cdot \beta^4 + 0.1944 \cdot \beta^8) \quad (20)$$

The obtained value was $C_c = 0.6006$.

Based on Fig. 12, it can be concluded that the values of coefficient C_e obtained in the experiment are close to the calculated value and are within the range of ± 1.39% resulting from the relative uncertainty from the standard [24]. The values of coefficient C_s obtained from the simulation are above the marked range, but their differences, compared to C_c, do not exceed 4.2%.

The results for the tested orifice confirm that the discharge coefficient is practically constant in the analysed range of Reynolds numbers (for the experiment from 9,900 to 16,300).

5. Conclusions

The article presents the results of simulation and experimental research for the segmental orifice with module $m = 0.25$ through which water flowed at the average temperature ranging from 20.7 °C to 24.8 °C (for each observed measurement series, the temperature change did not exceed 2.0 °C).

The simulations were performed using SolidWorks Flow Simulation 2014 for q_{ms} ranging from 0.25 kg/s to 0.65 kg/s. The calculations done in this software enable quick determination of pressure and velocity distributions within the tested orifice and its flow characteristics. The simulation results allow to reduce the costly and time-consuming experimental tests and facilitate the calibration and selection of instruments in the measurement path.

The investigation on the experimental stand was performed for seven different mass flow rates q_{me} ranging from 0.35 kg/s to 0.63 kg/s, which corresponded to Reynolds numbers in the range of 9,920 to 16,270. The experiments have shown that the obtained mass flow rate characteristic $q_{me} = f(\Delta p)$ is a power function with exponent 0.504, while according to the standard [24] the exponent value is only 0.5.

Compared to the standard-based calculations, the relative differences between the flow characteristics do not exceed 1.5% for the experiment and range from 5% to 5.1% for the simulation. The maximum relative mass flow rate difference between the simulation and experiment in the analysed range ofΔp does not exceed 6.5%, which is acceptable in industrial practice, where maintaining measurement conditions as stable as in the laboratory is very difficult.

The application of the analytical method and the Monte Carlo method in uncertainty analysis has shown that the highest value of relative expanded uncertainty obtained using these two methods did not exceed 1.8% and occurred for the lowest tested flow. At the same time, the relative expanded uncertainties obtained from the experimental calibration curve did not exceed 2.5%. This uncertainty value is considered a good result for mass flow measurements using orifices. On the other hand, from the calibration curve obtained from the simulations, the relative uncertainties have the largest values ranging from 3.87% to 4.43%. Due to the accuracy of the simulations performed, these values were considered too large.

After the study, the smallest values of relative uncertainty were obtained from the flow theory. In the case of uncertainty analysis of the flow obtained as a result of the simulations, due to the large uncertainty values (exceeding 4%), the mathematical model should be refined to show agreement with experiment and theory at a level not exceeding 1.5%. In the case of experimental calibration, the main difficulty is to maintain the same measuring conditions. Moreover, it is a labour-intensive and therefore costly method.

The obtained results of discharge coefficient *C* as a function of Reynolds number have shown that the tested segmental orifice is characterized by a stable value of this coefficient in the developing turbulent

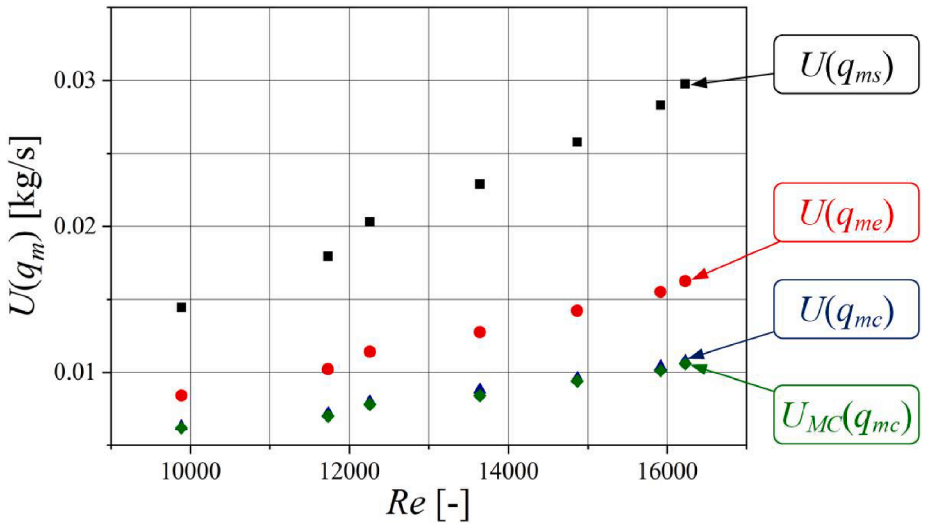

Fig. 11. Comparison of expanded mass flow rate uncertainties obtained from calculations, MC simulation, experiment and simulation calibration curves.

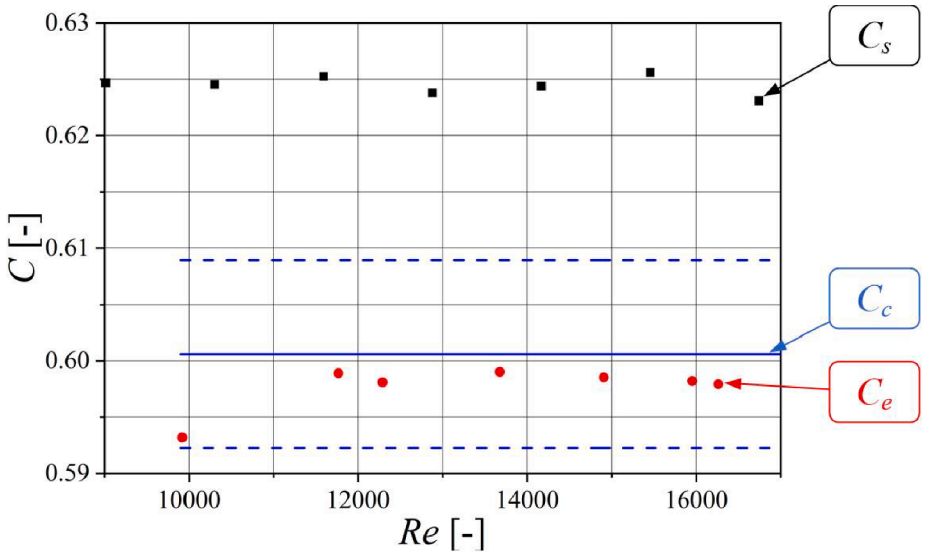

Fig. 12. Relationship between the discharge coefficient and the Reynolds number for experimental data and simulations.

flow (in the analysed range). That means that for this type of orifice, the coefficient C can be assumed constant for Reynolds numbers from 10,000, while the standard [22] describes this constancy for higher Re values, from 15,000.

The conducted analyses indicate that further research on the metrological properties of segmental orifices should be carried out. They should focus, among others, on improving the mathematical model of orifices, so that simulations show better agreement with experiment and theory.

CRediT authorship contribution statement

Anna Golijanek-Jędrzejczyk: Conceptualization, Methodology, Formal analysis, Writing - original draft, Writing - review & editing. **Andrzej Mrowiec:** Investigation, Resources, Validation, Writing - original draft. **Robert Hanus:** Formal analysis, Writing - review & editing. **Marcin Zych:** Formal analysis, Validation, Visualization, Writing - review & editing. **Marcin Heronimczak:** Visualization. **Dariusz Świsulski:** Writing - review & editing.

Declaration of Competing Interest

The authors declare that they have no known competing financial interests or personal relationships that could have appeared to influence the work reported in this paper.

Acknowledgements

This publication is partially supported by Polish Ministry of Education and Science under the program 'Regional Initiative of Excellence' in 2019 – 2022. Project number 027/RID/2018/19, funding amount 11 999 900 PLN. The publication is co-financed by the subsidy of the Department of Geophysics of the Faculty of Geology, Geophysics and Environmental Protection of AGH - University of Science and Technology. Subsidy number: 16.16.140.315.

References

[1] P. Gupta, K. Srinivasan, S.V. Prabhu, Tests on various configurations of Coriolis mass flowmeters, Measurement 39 (4) (2006) 296–307, https://doi.org/10.1016/j.measurement.2005.11.019.

[2] L.J. Wang, L. Hu, Z.C. Zhu, P. Ye, X. Fu, Analytical calculation of sensitivity for Coriolis mass flowmeter, Measurement 44 (6) (2011) 1117–1127, https://doi.org/10.1016/j.measurement.2011.03.011.
[3] T. Wang, R. Baker, Coriolis flowmeters: a review of developments over the past 20 years, and an assessment of the state of the art and likely future directions, Flow Meas. Instrum. 40 (2014) 99–123, https://doi.org/10.1016/j.flowmeasinst.2014.08.015.
[4] Y. Zhang, Y. Liu, Z. Liu, W. Liang, Developing a Long Short-Term Memory-based signal processing method for Coriolis mass flowmeter, Measurement 148 (2019), 106896, https://doi.org/10.1016/j.measurement.2019.106896.
[5] M. Viswanathan, A. Kandaswamy, S.K. Sreekala, K.V. Sajna, Development, modelling and certain investigations on thermal mass flow meters, Flow Meas. Instrum. 12 (5–6) (2002) 353–360, https://doi.org/10.1016/S0955-5986(02)00002-X.
[6] J. Dong, et al., Study on the measurement accuracy of an improved cemented carbide orifice flowmeter in natural gas pipeline, Flow Meas. Instrum. 99 (2018) 52–62, https://doi.org/10.1016/j.flowmeasinst.2017.12.008.
[7] N. Abed et al., 2020 IOP Conf. Ser.: Mater. Sci. Eng. 881 012050.
[8] Y.M. Yu, Z.H. He, H. Roesler, C. Solano, Z. Zhang, Design and application of thermal mass flow meter in space, NuclInstrum Methods Phys Res A. 950 (2020), 163003, https://doi.org/10.1016/j.nima.2019.163003.
[9] A. Golijanek-Jędrzejczyk, A. Mrowiec, R. Hanus, M. Zych, D. Świsulski, Uncertainty of mass flow measurement using centric and eccentric orifice for Reynolds number in the range 10,000 ≤ Re ≤ 20,000, Measurement 160 (2020), 107851, https://doi.org/10.1016/j.measurement.2020.107851.
[10] D. Kasprzak, A. Mrowiec, Analysis of the possibilities of measurement with eccentric orifice of flow medium for small Reynolds numbers, Pomiary Automatyka Robotyka 20 (2) (2016) 25–28, https://doi.org/10.14313/PAR_220/25. (in Polish).
[11] M. Jaszczur, A. Młynarczykowska, A general review of the current development of mechanically agitated vessels, Processes 8 (2020) 982, https://doi.org/10.3390/pr8080982.
[12] A. Andruszkiewicz, W. Wędrychowicz, P. Synowiec, P. Piechota, Analysis of the possibility of using an aperture in the pipeline as an orifice for continuous measurement of gas mass streams, Przegl. Elektrotech. 95 (11) (2019) 41–43, https://doi.org/10.15199/48.2019.11.10. (in Polish).
[13] B. Tomaszewska-Wach, M. Rzasa, B. Dobrowolski, O. Serediuk, Influence of the orifice shape on mass flow measurements of air–water mixture, WIT Transactions on Engineering Sciences; Southampton Vol 123, 33-42. Southampton: WIT Press 2019, DOI:10.2495/MPF190041.
[14] B. M. Levin, A. N. Lopatin, Measurement of the discharge of suspended mat-Ter-bearing flows in hydromechanization systems using segmental orifice plates, Izmeritel'nayaTekhnika, (1993) No. 6, 36-39.
[15] A. Mrowiec, M. Heronimczak, The research on the flow of incompressible fluid through selected segmented flange, Przegl. Elektrotech. 95 (11) (2019) 63–65, https://doi.org/10.15199/48.2019.11.16. (in Polish).
[16] M. Straka, C. Koglin, T. Eichler, Segmental orifice plates and the emulation of the 90°-bend, TeschnischesMessen 87 (1) (2020) 18–31.
[17] M. Straka, A. Fiebach, T. Eichler, C. Koglin, Hybrid simulation of a segmental orifice plate, Flow Meas. Instrum. 60 (2018) 124–133, https://doi.org/10.1016/j.flowmeasinst.2018.02.006.
[18] A. Buhidma, R. Pal, Flow measurement of two-phase oil-in-water emulsions using wedge meters and segmental orifice meters, The Chemical Engineering Journal and the Biochemical Engineering Journal 63 (1996) 59–64, https://doi.org/10.1016/0923-0467(95)03076-X.
[19] B.G. Liptak (Ed.), Process measurement and analysis, Chilton Book Company, 2003.
[20] G. Verma, SolidWorks Flow Simulation 2018 Black Book, Lightning Source Inc, CADCAMCAE Works, 2018.
[21] D. Taler, J. Sokołowski, Thermal measurements in industry, Agenda Wydawnicza PAK, Warszawa, 2006 (in Polish).
[22] EN ISO 5167-1: 2003 Measurement of fluid flow by means of pressure differential devices inserted in circular cross-section conduits running full - Part 1: General principles and requirements.
[23] EN ISO 5167-2: 2003 Measurement of fluid flow by means of pressure differential devices inserted in circular cross-section conduits running full - Part 2: Orifice plates.
[24] PN-93/M-53950/01 Pomiary strumienia masy i strumienia objętości za pomocą zwężek pomiarowych (Measurements of the mass flow and the volume flow by means of measuring orifices). (in Polish).
[25] Guide to the Expression of Uncertainty in Measurement, Joint Committee for Guides in Metrology (JCGM) 100:2008.
[26] J. Taylor, Introduction to error analysis the study of uncertainties in physical measurements, second edition, University Science Books, New York, 1997.
[27] A. Golijanek-Jędrzejczyk, D. Świsulski, R. Hanus, M. Zych, L. Petryka, Uncertainty of the liquid mass flow measurement using the orifice plate, Flow Meas. Instrum. 62 (2018) 84–92, https://doi.org/10.1016/j.flowmeasinst.2018.05.012.